Extremal Model for Amorphous Media Plasticity

Jean-Christophe Baret, Damien Vandembroucq, and Stéphane Roux

Unité Mixte CNRS/Saint-Gobain "Surface du Verre et Interfaces," 39 Quai Lucien Lefranc, 93303 Aubervilliers cedex, France

An extremal model for the plasticity of amorphous materials is studied in a simple two-dimensional antiplane geometry. The steady state is analyzed through numerical simulations. Long-range spatial and temporal correlations in local slip events are shown to develop, leading to nontrivial and highly anisotropic scaling laws. In particular, the plastic strain is shown to concentrate statistically over a region which tends to align perpendicular to the displacement gradient. By construction, the model can be seen as giving rise to a depinning transition, the threshold of which (i.e., the macroscopic yield stress) also reveals scaling properties reflecting the localization of the activity.

In contrast with crystalline solids, amorphous materials display a plasticity which cannot be attributed to the motion of well identified defects such as dislocations. Consequently, the microscopic description of amorphous plasticity still lacks a consistent framework. Recent studies [1–4] have focused on the fact that global plastic deformation is mostly due to local rearrangements. Starting from a molecular dynamics study of a bidimensional Lennard-Jones glass and measurements of the mechanical response under shear stress, Falk and Langer [1] introduced "shear transformation zones" having a bistable character to build a mean field theory of plastic deformation in an amorphous material. Initially applied by Bulatov and Argon [2–4] for amorphous solid materials, this approach can be extended to granular materials or dense suspensions [5,6].

In the following, we study a minimal model of plastic deformations in disordered media. This model was proposed in the early 1980s to describe the fault self-organization in seismic regions [7,8]. The "avalanche" properties of this model were studied in order to compare with the observed power-law distribution of seismic events (Gutenberg-Richter law). We show in the following that this very simple model reproduces the main features of plasticity in amorphous materials. The analysis we propose focuses on the scaling properties of the spatio-temporal organization of the local slip events and on the stress-strain characterization. We see that elementary slip events proceed through bursts of spatially localized activity, with a self-affine structure, forming bands at large scales. These bursts have a direct signature on the statistical distribution of macroscopic yield stress, which fluctuates in time. Part of this distribution [close to the maximum (over time) yield stress] displays a critical behavior characterized by a critical exponent (independent of the heterogeneity introduced in the model). The latter distribution rules the statistics of the noise (avalanches) which may be observed during plastic flow.

It is worth noting that the observation of nontrivial structures in plasticity has been the focus of a number of works based on very different approaches. At the microscopic scale, the patterning of dislocations in bands has been modeled by Selinger *et al.* [9]. Miguel *et al.* [10] studied the self-organization of dislocations during secondary creep. At a macroscopic level, Poliakov *et al.* [11,12] considered the patterning of slip bands of a solid obeying nonassociated plasticity under dynamic loading. However, for quasistatic loadings (or associated plasticity), most of the complexity of the plastic strain field vanishes. None of these approaches can be directly compared with the present study, in the sense that we resort to the microscopic scale and do not postulate any specific constitutive law (although one emerges naturally from our model) and that we do not build our description on dislocation dynamics.

We consider a bidimensional material submitted to antiplane shear stress. The only nonzero component of the displacement field $u_z(x, y)$ is along the z axis and it depends only on the plane coordinates. The material is discretized on a regular square lattice, the axes of which are oriented at 45° from the displacement gradient direction. Biperiodic boundary conditions are implemented for the stress and the strain. Hence, the displacement field $u_z(x, y)$ obeys $u_z(x, y + pL) = u_z(x, y) + p\varepsilon_{yz}L$ for any integer p, where L is the system size and ε_{yz} the imposed shear strain.

The medium is supposed to behave elastically (with a uniform shear modulus) up to a maximum shear stress, γ_{ij}, characterizing the yield limit of the interface between neighboring elements i and j. These local thresholds are randomly chosen from a uniform distribution between 0 and 1. Past the threshold, the interface is allowed to slip irreversibly along this specific interface by a random amount, Δu_{ij}. This displacement discontinuity gives rise to a new stress state in the entire medium computed using its elastic behavior. The local stress on an interface ij is $\sigma_{ij} = \Sigma + \sigma_{ij}^o$ where Σ is the macroscopic stress. After a slip Δu_{kl} at the interface kl, σ_i^o is adjusted to $\sigma_{ij}^o = \sigma_{ij}^o + \Delta u_{kl}G(x_{ij} - \underline{x_{kl}})$. Since the elastic modulus is uniform, the Green function G is computed once

and for all via a conjugated gradient algorithm for a unit slip at a reference interface. It is then simply translated to the location of the slip event. Apart from the periodicity imposed by the boundary conditions, this function $G(\underline{x})$ is long ranged, decreasing as $G(\underline{x}) \propto |\underline{x}|^{-2}$. Moreover, due to the shear boundary condition, the stress redistribution is anisotropic. In the longitudinal x direction, interfaces are loaded, while in the transverse y direction, they are unloaded. This anisotropy is one distinct feature of the model leading to the localization effect described below. Simultaneously, this slip is assumed to modify the local environment of the medium, and, hence, its limit stress is modified. A new threshold stress is thus chosen from the same distribution.

We choose an extremal dynamics: the external load is adjusted at each time step so that only one interface shear stress reaches its threshold. In terms of the global stress-strain characteristics of the system, one leaves an elastic branch to jump on another elastic branch of the same slope (the elastic modulus is uniform and is unchanged by the local slip) but whose origin has been shifted of $\Delta u_{ij}/L$.

The behavior of this model is of the pinning/depinning type. The yield criterion of an individual interface ij can be written $\Sigma^{ext} > \gamma_{ij} - \sigma_{ij}^{el}$, where Σ^{ext} is the external shear stress, γ_{ij} the local yield threshold, and σ_{ij}^{el} the local stress component due to elastic stress redistribution from previous yield events. Following an extremal dynamics, we select at time t the current "weakest interface" $i*$ such that $\sigma_c(t) = \gamma_{ij*} - \sigma_{ij*}^{el} = \min_{ij}[\gamma_{ij} - \sigma_{ij}^{el}]$. The current elastic limit $\sigma_c(t)$ is a fluctuating quantity. Its maximum over time $\sigma^* = \max_t \sigma_c(t)$ corresponds to the macroscopic yield stress. From this signal, we can reconstruct the evolution of the system subjected to a constant load: when submitted to an external shear stress lower than σ^*, the plate deforms plastically before blocking in a jammed state. For values above the yield stress, the system flows indefinitely. Such pinning systems have been extensively studied over the recent years. They have been used to describe front motion in a disordered environment in the context of wetting [13], magnetic domain walls [14], fluid invasion in porous media [15], crack propagation [16–18]; or the behavior of "periodic systems," e.g., vortex lattices [19] or charge density waves [20].

Beyond the yielding transition, this simple model exhibits another characteristic feature of plasticity: hardening (i.e., increase of the yield stress with the plastic strain). In crystalline solids, the hardening behavior is due to the entanglement or trapping on defects of dislocation loops. In the present case, after a first loading, we observe an increase of the elastic limit. However, the mechanism for this hardening effect is here of a pure statistical nature. During the loading process, the weakest sites are progressively decimated. Then the corresponding yield thresholds γ_{ij} are renewed. The new thresholds are in average larger than the previous ones. This introduces a systematical bias. When submitted for the first time to a

loading process, the distribution of these local yield thresholds evolves to eventually reach a stationary state. In Fig. 1, we show the evolution of the mean yield threshold $\langle \gamma_{ij} \rangle$ during loading. The asymptotic steady distribution seems not reached yet in the figure. This hardening effect thus corresponds to a progressive reinforcement of the weakest regions.

In Fig. 2 (top) we show a map of the cumulative plastic strain for a system of size 128×64 after 8×10^5 time steps. We see clearly that the plastic strain is nonuniform: it is localized within regions elongated along the x direction. Focusing on the plastic deformation taking place within a finite time window, we show in the same figure (bottom) the appearance of an individual localized structure. To characterize quantitatively this spatial distribution, we studied the pair correlation function of the plastic strain $\varepsilon_p(x, y)$ through Fourier transforms of the strain map averaged over time. We found that the projection of the plastic strain along the x or y axis, $\varepsilon_\parallel(x) = \langle \varepsilon_p(x, y) \rangle_y$ and $\varepsilon_\perp(y) = \langle \varepsilon_p(x, y) \rangle_x$, are self-affine profiles with roughness exponents $\zeta_\parallel \approx -0.09$ and $\zeta_\perp \approx 0.50$. Figure 3 shows the power spectra of ε_p for $k_x = 0$ and $k_y = 0$, where the power-law behaviors $|k|^{-1-2\zeta}$ give directly the cited roughness exponents.

Such a scaling behavior which characterizes the steady-state fluctuations of the cumulative strain allows one to analyze the time evolution of the plastic flow. Let us consider two local slip events separated by a time lapse τ and record their distance along the x and y directions, noted respectively as $d_\parallel$ and $d_\perp$. Averaging over time (at fixed τ), the probability distribution function of these distances $p(d, \tau)$ reveal two characteristic "correlation lengths," $\xi_\parallel$ and $\xi_\perp$, below which p is constant, and above which p decays as a power law with an exponent $\alpha_\parallel$ or $\alpha_\perp$, respectively. Varying the time lapse τ, we observe that
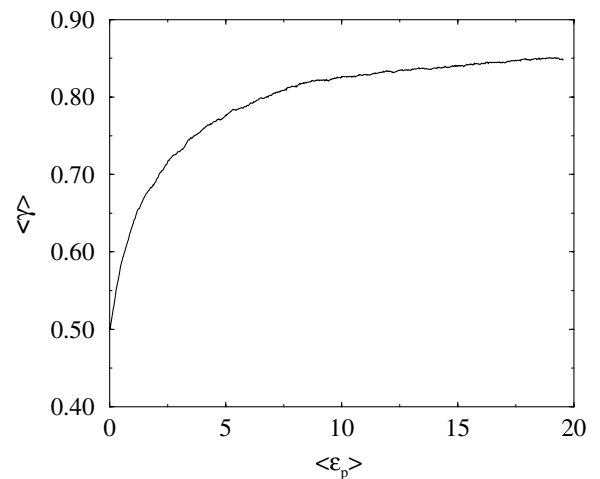
FIG. 1. Evolution of the mean yield threshold $\langle \gamma \rangle$ versus the plastic strain $\langle \varepsilon_p \rangle$ during the transient regime of a first loading process. The increase of $\langle \gamma \rangle$ can be interpreted as a hardening effect.
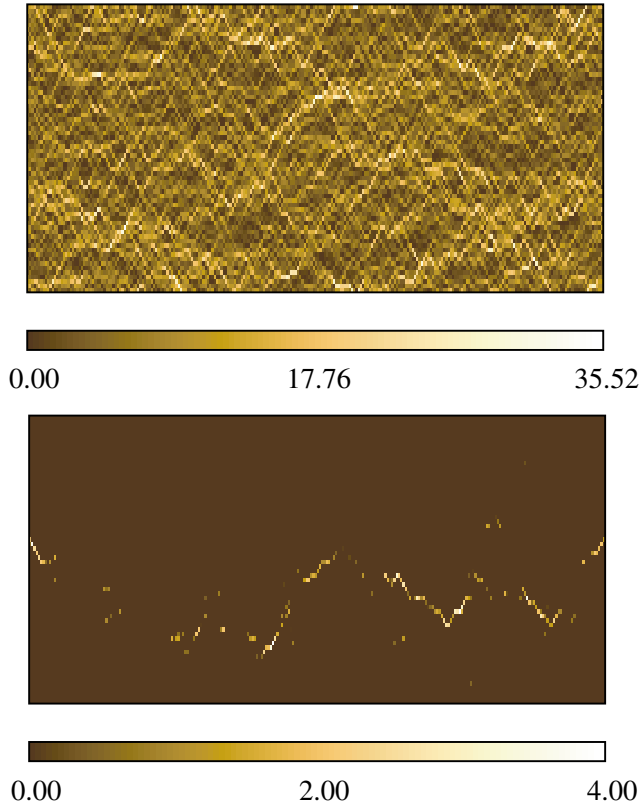
FIG. 2 (color online).   Map of the relative displacement field obtained on a system 128×64 after $800\,000$ time steps (top). The diffuse localization corresponds to the successive development of anisotropic structures elongated in the longitudinal direction. Focusing on a finite time window (450 time steps, bottom) allows one to reveal an individual structure.

$$\xi_\parallel(\tau) \propto \tau^{1/z_\parallel}, \qquad \xi_\perp(\tau) \propto \tau^{1/z_\perp}. \qquad (1)$$

Exploiting the self-affine nature of the cumulative plastic strain, and using a result obtained for other extremal models of depinning, we can relate the two dynamic exponents to the roughness exponents [21]. During a time lapse τ, most of the activity takes place in a region of extension ξ, the difference between the front and time t, and $t + \tau$ is a self-affine region of lateral extension ξ of typical width ξ^ζ and of area τ. The equality $\xi \cdot \xi^\zeta = \tau$ leads to

$$z_\parallel = 1 + \zeta_\parallel, \qquad z_\perp = 1 + \zeta_\perp. \qquad (2)$$

The numerical values of the z exponents are consistent with these identities.

The difference in scaling in the x and y directions can be accounted for through a power law relating to both directions. Indeed, the correlation lengths are related through $\xi_\perp \propto \xi_\parallel^\beta$ with $\beta = z_\parallel/z_\perp \approx 0.65$. Moreover, looking at the mean value of $d_\perp$ for a prescribed value of $d_\parallel$ also reveals the same power law $d_\perp \propto d_\parallel^\beta$, with $\beta \approx 0.65$.
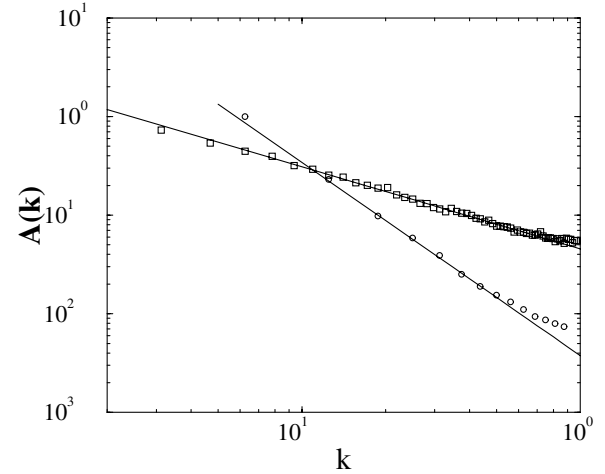
FIG. 3.   Power spectra of the plastic strain ε_p for $k_x = 0$ (circles) and $k_y = 0$ (squares). The lines indicate power-law behaviors corresponding to roughness exponents $\zeta_\parallel = -0.09$ and $\zeta_\perp = 0.50$.

Let us focus now on the depinning stress distribution. Prior to a large jump in the location of the slip event, the lattice has reached a state of strong pinning. Hence, following the analysis presented in Ref. [22], if we condition the statistical distribution of $\sigma_c(t)$ by the distance to the location of the next slip event, along the x direction for instance, Δx, we observe that the larger Δx, the narrower the distribution and the closer its mean to the yield stress σ^*. These distributions are shown in Fig. 4. Motivated by the underlying criticality of the depinning transition, we may anticipate a scaling form of the distribution as

$$p(\sigma_c \mid \Delta x) = \Delta x^{\nu_\parallel} \psi[(\sigma^* - \sigma_c)\Delta x^{\nu_\parallel}]. \qquad (3)$$

This particular form implies that the standard deviation of the distribution $\delta\sigma_c$ vanishes as $(\Delta x)^{-\nu_\parallel}$ and that the mean value of $\langle \sigma^* - \sigma_c \rangle (\Delta x)$ is simply proportional to $\delta\sigma_c(\Delta x)$. The first property allows one to determine $\nu_\parallel$ and the second gives a simple way to estimate precisely σ^* through a simple linear regression. The same procedure applied to Δy gives a similar result. Using the linear dependence of $\delta\sigma_c$ on σ_c conditioned to the size of the activity jump in both the x and y directions, we find numerically $\sigma^* \approx 0.517$ for a uniform distribution of threshold γ in $[0, 1]$ and a random slip amplitude from the same distribution.

The scaling of the standard deviation of the distribution versus the jump size gives a determination of the exponents $\nu_\parallel \approx 0.68$ and $\nu_\perp \approx 0.98$. We note that again the ratio of these exponents gives the anisotropy scaling $\beta = \nu_\parallel/\nu_\perp = 0.69$ in good agreement with the previous determinations ($\beta \approx 0.65$).

The knowledge of the distribution $p(d) \propto d^{-\alpha_\parallel}$ of the x distances between successive active sites allows one to express the depinning stress distribution close to
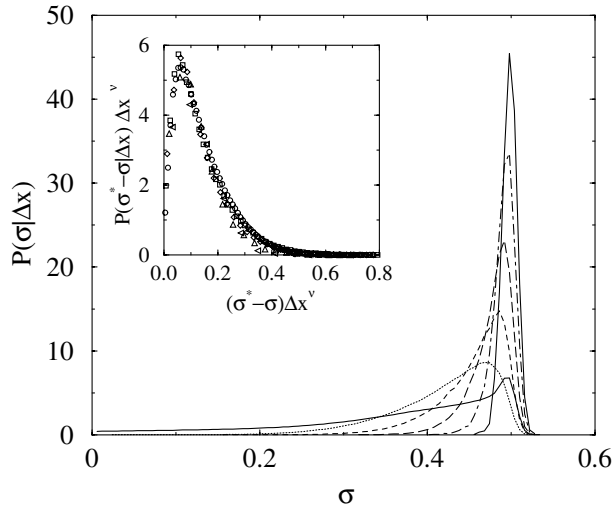
FIG. 4. Distribution of depinning stress (bold line) and contributions conditioned by the distances (2, 4, 8, 16, 32) between consecutive active sites. The tail of the distribution corresponds to very short jumps and is very sensitive to the details of the random threshold distribution. The contributions obtained for increasing distances between consecutive active sites present the same trend: the larger the jump, the closer the mean force to the threshold and the narrower the distribution. After rescaling (inset) these distributions collapse onto a single master curve.

threshold:

$$\mathcal{Q}(\sigma^* - \sigma_c) = \int x^{\nu_\parallel - \alpha_\parallel} \psi\!\left(\frac{\sigma^* - \sigma_c}{x^{-\nu_\parallel}}\right) dx \propto (\sigma^* - \sigma_c)^\mu,$$

where $\mu = (\alpha_\parallel - \nu_\parallel - 1)/\nu_\parallel$. The same argument obviously also holds for the y direction. This latter scaling is also consistent with the anisotropy scaling $\beta = (\alpha_\parallel - 1)/(\alpha_\perp - 1) \approx 0.64$.

Despite its extreme simplicity, the model that we present accounts for several features of plasticity in amorphous materials. We could identify a macroscopic yield stress. Below this threshold, the material deforms elastically before blocking in a jammed state. Above, it can flow indefinitely. This behavior is typical of a pinning/depinning situation. In the same spirit as the study presented in Ref. [22], the model exhibits a critical behavior of the plastic stress close to the macroscopic yield stress. When submitted for the first time to a shear stress, we observe a hardening effect. In contrast with crystalline materials, here this effect is of a pure statistical nature and corresponds to a progressive reinforcement of the weakest regions. In addition to this global hardening plastic behavior, the model exhibits a statistical localization. The latter appears via elongated structures in the shear direction. However, instead of concentrating on a unique structure (such as in Ref. [8]), the plastic strain develops a complex spatiotemporal organization. A statistical analysis of these patterns reveals scaling properties; scaling exponents are summarized in Table I.

TABLE I. Table of scaling exponents.

$\zeta_\parallel = -0.09 \pm 0.10$	$\zeta_\perp = 0.50 \pm 0.05$
$\alpha_\parallel = 1.61 \pm 0.10$	$\alpha_\perp = 1.96 \pm 0.10$
$\nu_\parallel = 0.68 \pm 0.05$	$\nu_\perp = 0.98 \pm 0.05$
$\mu = 0.00 \pm 0.10$	$\beta = 0.65 \pm 0.05$

Beyond this simplified model, the introduction of thermal activation in the selection of the site to plastify should allow one to account for viscoplastic effects. Another improvement of such models would consist in including both deviatoric and volumetric strain, the latter coupling being characteristic of irreversible deformation in amorphous solids.

[1] M. L. Falk and J. S. Langer, Phys. Rev. E **57**, 7192 (1998).
[2] V. V. Bulatov and A. S. Argon, Model. Simul. Mater. Sci. Eng. **2**, 167 (1994).
[3] V. V. Bulatov and A. S. Argon, Model. Simul. Mater. Sci. Eng. **2**, 185 (1994).
[4] V. V. Bulatov and A. S. Argon, Model. Simul. Mater. Sci. Eng. **2**, 203 (1994).
[5] A. Lemaître, Phys. Rev. Lett. **89**, 064303 (2002).
[6] A. Lemaître, cond-mat/0108442 [Phys. Rev. Lett. (to be published)].
[7] K. Chen, P. Bak, and S. P. Obhukhov, Phys. Rev. A **43**, 625 (1991).
[8] P. Miltenberger, D. Sornette, and C. Vanneste, Phys. Rev. Lett. **71**, 3604 (1993).
[9] R. L. B. Selinger, B. B. Smith, and W. D. Luo, Mater. Res. Soc. Symp. Proc. **653**, Z5.4 (2000).
[10] M. C. Miguel, A. Vespignani, M. Zaiser, and S. Zapperi, Phys. Rev. Lett. **89**, 165501 (2002).
[11] A. N. B. Poliakov and H. J. Herrmann, Geophys. Res. Lett. **21**, 2143 (1994).
[12] A. N. B. Poliakov, H. J. Herrmann, Y. Y. Podlachikov, and S. Roux, Fractals **2**, 567 (1994).
[13] E. Rolley, C. Guthmann, and R. Gombrowicz, Phys. Rev. Lett. **80**, 2865 (1998).
[14] S. Lemerle, J. Ferré, C. Chappert, V. Mathet, T. Giamarchi, and P. Le Doussal, Phys. Rev. Lett. **80**, 849 (1998).
[15] D. Wilkinson and J. F. Willemsen, J. Phys. A **16**, 3365 (1983).
[16] J. Schmittbuhl, S. Roux, and Y. Berthaud, Europhys. Lett. **28**, 585 (1994).
[17] A. Tanguy, M. Gounelle, and S. Roux, Phys. Rev. E **58**, 1577 (1998).
[18] S. Ramanathan and D. S. Fisher, Phys. Rev. B **58**, 6026 (1998).
[19] G. Blatter, M. V. Feigel'man, V. B. Geshkenbein, A. I. Larkin, and V. M. Vinokur, Rev. Mod. Phys. **66**, 1125 (1994).
[20] G. Grüner, Rev. Mod. Phys. **60**, 1129 (1988).
[21] When $\zeta < 0$, an effective value of $\zeta^{\text{eff}} = 0$ should be read in this formula.
[22] R. Skoe, D. Vandembroucq, and S. Roux, Int. J. Mod. Phys. C **13**, 751 (2002).